erably modified for the nonplanar MOETPPs in comparison with planar MOEP and MTPP counterparts. In particular, the dependence of ν_2 and ν_3 on core size is greatly decreased for the nonplanar porphyrins. Such spectral relationships are often useful in structure–function correlations in molecular biology and play a central role in the use of Raman spectroscopy in studies of the chemical and photochemical function of tetrapyrrole cofactors in proteins and in other chemical environments. Relationships among the frequencies of structure-sensitive Raman lines and two structural parameters, porphyrin core size and C_α–N–C_α angle, have been analyzed for the MOETPP series. The MOETPPs show only weak variation in Raman frequencies in spite of large differences in core size (0.15 Å) for the series of metals employed. This behavior contrasts sharply with those of the metal TPPs and OEPs which exhibited a strong metal dependence over this range of core sizes. On this basis core size does not determine the frequency of the structure-sensitive Raman lines. On the other hand, the frequency dependence on the C_α–N–C_α angle, which varies only over a small range (2°) for the MOETPPs, is comparable (within the uncertainties in the slope) to that for the MOAPs.

Porphyrin optical transitions are also affected by deviations from planarity. INDO/CI molecular orbital calculations can accurately predict the trends in the $\pi \rightarrow \pi^*$ transitions for a series of nickel porphyrins with varying nonplanarity if the structures obtained from molecular mechanics are used in the MO calculations. However, accurate prediction of the transition energies also requires the inclusion of all macrocycle substituents in the MO calculations.

In summary, the results presented here and elsewhere demonstrate that molecular mechanics calculations can be used to predict the structures of highly substituted porphyrins, including the structural effects of different substituents and metal ions and the degree of nonplanarity[9-11] and the type of nonplanar distortion.[14b] Clear relationships are observed between the metal present in the porphyrin and structural parameters determined by resonance Raman, optical absorption, and NMR spectroscopy.[7,9-11,14] This information is currently being used in the molecular design of nonplanar pocket porphyrins as biomimetic catalysts.

Acknowledgment. We thank K. M. Barkigia and J. Fajer for communicating their results for the X-ray crystal structure of NiOETPP prior to publication. Work performed at Sandia National Laboratories was supported by the U.S. Department of Energy Contract DE-AC04-76DP00789 (J.A.S.). Work performed at the University of California was supported by the National Science Foundation Grant CHE-90-01381 (K.M.S.) and the Deutsche Forschungsgemeinshaft Se 543/1-1 (M.O.S.). C.J.M. thanks the Fulbright Commission for the award of a Travel Scholarship and L.D.S. thanks the Associated Western Universities for a Graduate Fellowship.

Supplementary Material Available: Labeling scheme for CoOETPP and details of the crystal structure determinations of CoOETPP and CuOETPP including lists of atomic coordinates, anisotropic thermal parameters, H-atom coordinates, bond lengths, bond angles, torsion angles, and least-squares planes (31 pages); listing of observed and calculated structure factors (88 pages). Ordering information is given on any current masthead page.

Chemical and Electrochemical Investigation of Redox-Associated Conformational Changes in the Bis(1,4,7-trithiacyclononane)copper(II/I) System and X-ray Structure of the Copper(I) Complex

Sanaullah, Kenji Kano,[†] Richard S. Glass,[‡] and George S. Wilson*

Contribution from the Department of Chemistry, The University of Kansas, Lawrence, Kansas 66045. *Received July 15, 1992*

Abstract: Extensive electrochemical measurements of the kinetic parameters for electron transfer in aqueous bis(1,4,7-trithiacyclononane)copper(II) ($[Cu^{II}(TTCN)_2]$) and its Cu(I) analog have been carried out at a glassy carbon electrode. Our studies have shown that the $[Cu^{II}(TTCN)_2]/[Cu^{I}(TTCN)_2]$ system follows an ECEC square mechanism rather than just simple electron transfer as suggested previously. Unlike the octahedral Cu(II) complex, $[Cu(TTCN)_2]PF_6$ crystallizes with two independent formula units in space group $P2_1/n$ of the monoclinic system with unit cell dimensions a = 8.608 (3) Å, b = 31.041 (8) Å, c = 16.008 (4) Å, and β = 90.88 (2)°. The two molecular units have distorted tetrahedral CuS_4 coordination spheres with monodentate and tridentate TTCN ligands. The mondentate ligands have a unique conformation for the TTCN moiety with Cu(I) coordinated differently in each of the two independent $[Cu^{I}(TTCN)_2]$ units. The ring conformation, however, remains the same. The uncoordinated sulfur atoms on the monodentate TTCN ligand can coordinate to a metal ion added to the solution, and this ligand ultimately reverts to a tridentate ligand with the standard endodentate [3 3 3] conformation of the TTCN moiety. The transient trinuclear complex with added Cu(II) can be detected both electrochemically and spectrophotometrically. Electrochemical oxidation of $[Cu^{I}(TTCN)_2]$ and reduction of $[Cu^{II}(TTCN)_2]$ both occur rapidly, but in both cases, the electron transfer is followed by chemical steps. These chemical steps are the conformational reorganization of the monodentate TTCN ligand into the tridentate [3 3 3] conformer and the reverse of this process, respectively. Digital simulations of the cyclic voltammetric data for the kinetic parameters of both the $[Cu^{II}(TTCN)_2]/[Cu^{I}(TTCN)_2]$ system and the entire mechanism of the interaction between $[Cu^{I}(TTCN)_2]$ and Cu(II) followed by the subsequent reduction of the intermediate have been carried out.

Introduction

Despite the significantly different coordination geometries of Cu(II) and Cu(I) cations, a number of copper proteins involved in electron transport in biological systems accommodate these differences. This has inspired research directed toward characterization of the metal center. The facile electron transfer in these proteins has been accomplished (i) by geometrical preorganization of the metal-binding site in a near-entatic state and (ii) by an exquisite selection of the ligand system about the metal center such that both the oxidized and reduced states will be stabilized.[1]

[†] Gifu Pharmaceutical University, 5-6-1 Mitahora-Higashi, Gifu 502, Japan.
[‡] Department of Chemistry, The University of Arizona, Tucson, AZ 85721.

(1) Colman, P. M.; Freeman, H. C.; Guss, J. M.; Murata, M.; Norris, V. A.; Ramshaw, J. A. M.; Venkatappa, M. P. *Nature (London)* **1978**, *272*, 319.

0002-7863/93/1515-592$04.00/0

The disputed involvement of the thioether ligand from methionine in the electron-transfer process of blue copper proteins[2] has prompted a high level of interest in the synthesis of model compounds and in the kinetics and mechanisms of the redox reactions of these compounds.[3] It is almost impossible for copper proteins to be exactly mimicked; however, the rigidity of the inner sphere can be achieved by using macrocyclic ligands of appropriate ring size. This approach would be especially useful for thioether ligands because of their poor coordination capability.[4] The macrocyclic effect has played the most important role in coordinating crown thioethers to a wide variety of metal atoms, sometimes with very unusual oxidation states.[5,6]

Although the homoleptic thioether complexes are clearly not models for the blue copper proteins, their redox chemistry has provided very useful information about the electron-transfer reactions involving copper–thioether coordination.[7]

In view of the stereochemical preferences of Cu(II) and Cu(I), the reversibility of electron transfer can be improved by restricting the flexibility of the macrocycles, but at the same time, the macrocycle should also be amenable to coordination with both Cu(II) and Cu(I).

The X-ray crystallographic data of 1,4,7-trithiacyclononane (TTCN) have shown the molecule to adopt a [3 3 3] conformation with all three sulfur atoms *endodentate*,[8] preorganizing the ligand for facial coordination with metal atoms. Both condensed- and gas-phase studies have shown that the molecule retains this structure.[8,9] This has been further supported by the cyclic voltammetric data of a number of metal complexes with TTCN.[10] The electrochemical reversibility in the $[Cu^{II}(TTCN)_2]/[Cu^{I}(TTCN)_2]$ system has been ascribed so far to the minimal reorganization of the metal ion coordination as a consequence of the structural rigidity of TTCN.[11]

The propensity of the TTCN macrocycle to retain the endodentate [3 3 3] conformation is also evident from the fact that, with the exception of one or two cases, the metal atom receives more than one bite from the same TTCN macrocycle. In $[Au^{I}(TTCN)_2]$, one of the TTCN units is shown to act as a mondentate ligand, and this has been ascribed to a compromise between two extreme stereochemical tendencies at the metal center, ~~he~~. linear on the part of Au(I) and tetrahedral on the part of the ligand.[12] Clarkson et al. in 1989 reported the crystal structure of a binuclear copper–TTCN complex ($[Cu^{I}_2(TTCN)_3]$) in which two Cu(I) centers, each one capped by a terminal TTCN molecule, are bridged by a central TTCN molecule, showing that the bridging TTCN molecule no longer retains its endodentate [3 3 3] conformation.[13] The conformation adopted by the monodentate TTCN ring in the Au(I) complex and the bridging TTCN ligand in the Cu(I) complex is the same [1 2 2 2 2] conformation (with a local approximate C_2 axis of symmetry).

In the present work, we have shown electrochemically that TTCN can also undergo conformational changes to adjust to the geometrical requirements of the corresponding oxidation state of the central metal atom. The conformation of the monodentate ligand can even be utilized for further coordination with another suitable metal ion to the available sulfur atoms for a short period of time.

Table I. Crystal Data[a] for $[Cu(TTCN)_2]PF_6$

mol formula	$CuC_{12}H_{24}S_6PF_6$
fw	569.19
space group	$P2_1/n$ (No. 14)
a, Å	8.608 (3)
b, Å	31.041 (8)
c, Å	16.008 (4)
β, deg	90.88 (2)
V, Å^3	4277 (4)
Z	8
d_{calcd}, g cm^{-3}	1.768
crystal color, shape	colorless, plate
crystal dimensions, mm	0.30 × 0.20 × 0.05
no. of unique data	5741
no. of obsd data	2792
μ (Cu Kα), cm^{-1}	80.46

[a] Standard deviation of the least significant figure is given in parentheses.

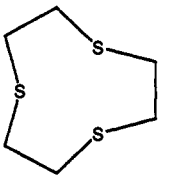

L: TTCN

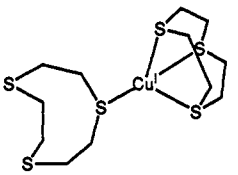

ML: $[Cu^{I}(TTCN)_2]$

Experimental Section

Instrumentation. Electrochemical experiments were carried out using a computer-controlled Cypress electroanalytical system, Model CS-1090. A Princeton Applied Research (PAR) Model 273 potentiostat/galvanostat equipped with a digital coulometer was used for the controlled-potential electrolysis (CPE) and chronocoulometric experiments.

The potentials were measured against a Ag/AgCl (saturated NaCl) reference electrode. The auxiliary electrode consisted of a large platinum flag, and the working electrode consisted of glassy carbon press-fitted into a Kel-F shroud (Bioanalytical Systems). The latter was used for stationary electrode voltammetry, and a Pine Instruments Model AFDTO6GCPT glassy carbon disk–platinum ring electrode was used for the RDE.

All the experiments were performed in a three-compartment cell separated by medium-porosity frits and $NaNO_3$ salt bridges. No correction was made for the liquid junction potential.

Electronic spectra were recorded on a Cary Model 219 UV-visible-recording spectrophotometer.

Reagents. All the chemicals employed were from Aldrich and were used as obtained. The complex $[Cu(TTCN)_2](BF_4)_2$ was prepared according to the literature method.[14] $Cu(NO_3)_2$ was used for preparing the free-copper solutions. The solutions were prepared in a 0.1 M sodium tetrafluoroborate solution. The pH of the $NaBF_4$ solution was adjusted to 3 with a few drops of tetrafluoroboric acid. High-purity 18-MΩ water was used for preparing all the solutions. Tetrakis(acetonitrile)copper(I) hexafluorophosphate ($[Cu(CH_3CN)_4]PF_6$) was prepared according to the reported method.[15]

Preparation of $[Cu(TTCN)_2]PF_6$. The synthetic procedure recommended by Clarkson et al.[13] was adapted for synthesis of the title complex. To a solution of 1,4,7-trithiacyclononane (500 mg, 2.77 mmol) in methanol (50 mL, Aldrich sure seal) under argon was added $[Cu(CH_3CN)_4]PF_6$ (500 mg, 1.34 mmol). The reaction mixture was stirred under argon for about 2 h, and the resulting white precipitate was filtered off and washed sequentially with methanol, ethanol, and finally diethyl ether under argon.

The above product was dissolved in 1–2 mL of nitromethane which was prepurged with argon. A 20-mL portion of methanol was added slowly and allowed to mix slowly with the solution in a refrigerator. The

(2) Solomon, E. I.; Gewirth, A. A.; Cohn, S. L. *ACS Symp. Ser.* **1986**, *307*, 236.
(3) Karlin, K. D., Zubieta, J., Eds. *Biological and Inorganic Copper Chemistry*; Adenine Press: New York, 1986; Vol. 2.
(4) Murray, S. G.; Hartley, F. R. *Chem. Rev.* **1981**, *81*, 365.
(5) Westerby, B. C.; Juntunen, K. L.; Leggett, G. H.; Pett, V. B.; Koenigbauer, M. J.; Purgett, M. D.; Taschner, M. J.; Ochrymowycz, L. A.; Rorabacher, D. B. *Inorg. Chem.* **1991**, *30*, 2109 and references therein.
(6) Blake, A. J.; Schroder, M. In *Advances in Inorganic Chemistry*; Sykes, A. G., Ed.; Academic Press: New York, 1990; Vol. 35, p 1.
(7) Rorabacher, D. B.; Martin, M. J.; Koenigbauer, M. J.; Malik, M.; Schroeder, R. R.; Endicott, J. F.; Ochrymowycz, L. A. In *Copper Coordination Chemistry: Biochemical and Inorganic Perspectives*; Karlin, K. D., Zubieta, J., Eds.; Adenine Press: New York, 1983; p 167.
(8) Glass, R. S.; Wilson, G. S.; Setzer, W. N. *J. Am. Chem. Soc.* **1980**, *102*, 5068.
(9) Setzer, W. N.; Coleman, B. R.; Wilson, G. S.; Glass, R. S. *Tetrahedron* **1981**, *37*, 2743.
(10) Swanson, D. D. Ph.D. Thesis, University of Arizona, 1985.
(11) Cooper, S. R.; Rawle, S. C. *Struct. Bonding (Berlin)* **1989**, *72*, 1.
(12) Blake, A. J.; Gould, R. O.; Greig, J. A.; Holder, A. J.; Hyde, T. I.; Schroeder, M. *J. Chem. Soc., Chem. Commun.* **1989**, 876.
(13) Clarkson, J. A.; Yagbasan, R.; Blower, P. J.; Cooper, S. R. *J. Chem. Soc., Chem. Commun.* **1989**, 1244.
(14) Setzer, W. N.; Ogle, C. A.; Wilson, G. S.; Glass, R. S. *Inorg. Chem.* **1983**, *22*, 266.
(15) Kabus, G. J. In *Inorganic Synthesis*; Shriver, D. F., Ed.; Wiley-Interscience: New York, 1979; Vol. 19, p 90.

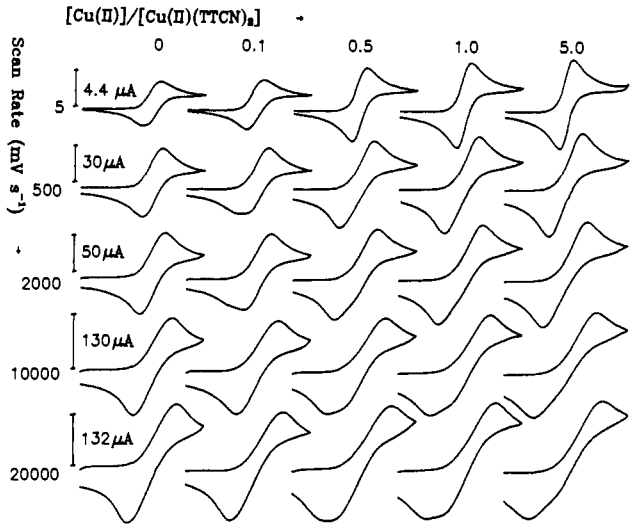

Figure 1. Variation in the cyclic voltammograms of 1.0 mM [Cu^{II}(TTCN)$_2$] as a function of free Cu(II) concentration and scan rate (v).

volume was then reduced on a rotary evaporator to about 3 mL, and the microcrystalline product was filtered off and washed as described above. The yield was 90%.

Anal. Calcd for $C_{12}H_{24}S_6CuPF_6$: C, 25.32; H, 4.25; S, 33.79; F, 20.02. Found: C, 25.24; H, 4.11; S, 33.62; F, 19.73.

X-ray Single-Crystal-Structure Study of [Cu(TTCN)$_2$]PF$_6$. Recrystallization of [Cu(TTCN)$_2$]PF_6 from acetonitrile by slow evaporation under a gentle stream of argon gave colorless plates. A crystal having approximate dimensions of 0.30 × 0.20 × 0.50 mm was mounted on a Rigaku AFC5R diffractometer. Cu Kα radiation (λ = 1.541 78 Å) was used with a graphite monochromator and a 12-kW rotating-anode generator. The automatic centering and least-squares routines were carried out on 25 reflections in the 2θ range, 30.6–48.4°, and the cell constants determined by least-squares refinement of these reflections are given in Table I. The monoclinic space group was determined from systematic absences to be $P2_1/n$ (No. 14). The (ω–2θ) data collection technique was used, and data were collected to a maximum 2θ of 112.5°.

Of the 6205 reflections which were collected, 5741 were unique (R_{int} = 0.147). The intensities of three representative reflections which were measured after every 150 reflections declined by 15.00%. A linear correction factor was applied to the data to account for this phenomenon.

The linear absorption coefficient for Cu Kα is 80.5 cm^{-1}. An empirical absorption correction using the program DIFABS[16] was applied which resulted in transmission factors ranging from 0.95 to 1.00. The data were corrected for Lorentz and polarization effects.

The structure was solved by a combination of the Patterson method[17] and direct methods.[18] The non-hydrogen atoms were refined anisotropically. The structure was refined by full-matrix least-squares techniques by using neutral-atom scattering factors,[19] and anomalous dispersion terms[20] were included in F_c; the values for $\Delta f'$ and $\Delta f''$ were those of Cromer.[21] All calculations were performed using the TEXSAN[22] crystallographic software package of the Molecular Structure Corp. The structure of the complex showed considerable disorder especially of the singly coordinated macrocyclic ring. The refinement showed two discrete structural units. This disorder in the structure prevented refinement to an R factor lower than 0.089. The final cycle of refinement included 469 variables and converged with unweighted and weighted agreement factors of 0.089 and 0.136, respectively. The highest peak in the final difference Fourier had a height of 1.18 e/Å^3. The goodness-of-fit indicator was 2.21.

The final thermal displacement parameters, together with full tables of bond distances and angles, are available in the supplementary material.

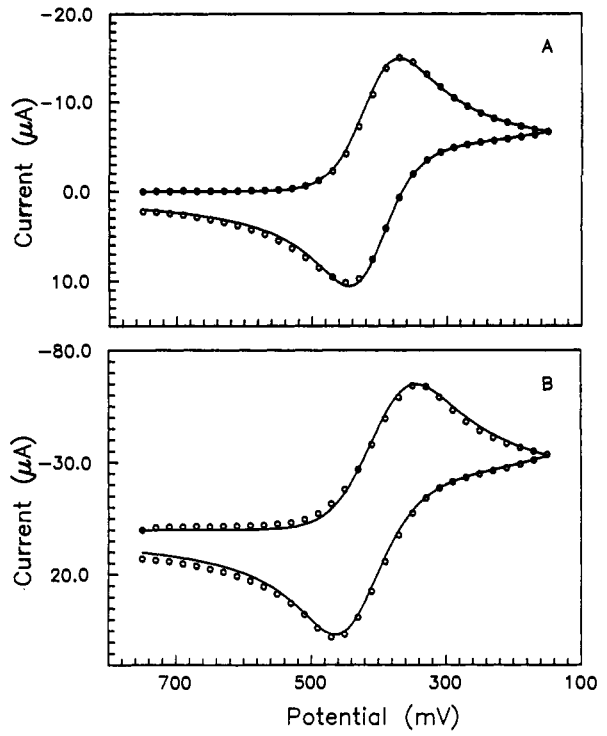

Figure 2. Background-corrected experimental (∞) and corresponding digitally simulated (—) cyclic voltammograms of 1.0 mM [Cu^{II}(TTCN)$_2$] at scan rates of (A) 0.100 V s^{-1} and (B) 1.500 V s^{-1}. $E^{\circ\prime}_1$ = 0.408 V, α_1 = 0.45, and k_{sh1} = 0.0134 cm s^{-1}.

Digital Simulation of the Cyclic Voltammograms. The normal explicit finite-difference digital-simulation technique[23] was employed in the calculation of current–potential curves. The calculation internal (ΔE_{calc}) was 1 mV unless otherwise stated. The experimental current–potential (i–E) data acquired on the Cypress system were corrected for the background currents every 5 mV. In the curve-fitting analysis of voltammograms, the dumping Gauss–Newton method[24] was applied as a nonlinear least-squares technique. All computer programs were written in Turbo Pascal. The calculations were carried out on a Gateway 2000 VGA 386 or an NEC PC-9801RA microcomputer equipped with a math coprocessor. Digital simulation and curve-fitting analysis of the cyclic voltammograms have previously been described.[25]

Results and Discussion

Electrochemistry of the [Cu^{II}(TTCN)$_2$] Complex. Figure 1 summarizes the electrochemistry of the [Cu^{II}(TTCN)$_2$] complex at various scan rates and in the presence of added Cu(II). Column 1 in Figure 1 shows a number of voltammograms of 1 mM [Cu^{II}(TTCN)$_2$] at different scan rates (no added Cu(II)). The cyclic voltammetric (CV) data show only one well-defined electron-transfer step at all scan rates examined up to 135 V s^{-1}. The CV curves at a scan rate (v) less than 10 mV s^{-1} are practically reversible with an $E^{\circ\prime}$ of 408 ±2 mV vs Ag/AgCl. With increasing scan rate, however, the peak separation (ΔE) increases due to the finite electron-transfer rate and/or increased solution resistance. The invariance of the shape of the cyclic voltammograms indicates consistent mechanistic characteristics of the electron-transfer process over the range of experimental conditions employed, especially the time scale of the experiment.

Both the reduction of [Cu^{II}(TTCN)$_2$] as well as the oxidation of [Cu^{I}(TTCN)$_2$] at the RDE at a scan rate of 5 mV/s and a rotation speed (f') of 25 rpm produced the typical sigmoidal i–E curves. Levich plots (i_{lim} vs $\omega^{1/2}$, where $\omega = 2\pi f'/60$) afforded straight lines for both cathodic and anodic processes up to 3600

(16) Walker, N.; Stuart, D. *Acta Crystallogr.* **1983**, *A39*, 158.
(17) Calbrese, J. C. Ph.D. Thesis, University of Wisconsin, 1972.
(18) Beurskens, P. T. *Technical Report 1984/I; Crystallography Laboratory: Toernooiveld, 6525 Ed* Nijmegen, The Netherlands, 1984.
(19) Cromer, D. T.; Waber, J. T. *International Tables for X-ray Crystallography*; The Kynoch Press: Birmingham, England, 1974; Vol. IV, Table 2.2 A.
(20) Ibers, J. A.; Hamilton, W. C. *Acta Crystallogr.* **1964**, *17*, 781.
(21) Cromer, D. T. *International Tables for X-ray Crystallography*; The Kynoch Press: Birmingham, England, 1974; Vol. IV, Table 2.3.1.
(22) *TEXSAN-TEXRAY Structure Analysis Package*; Molecular Structure Corp.: Woodlands, TX, 1985.
(23) Feldberg, S. W. In *Electroanalytical Chemistry*; Bard, A. J., Ed.; Marcel Dekker: New York, 1969; Vol. 3, p 199.
(24) Kowalik, J.; Osborne, M. R. *Methods for Unconstrained Optimization Problems*; Elsevier: Amsterdam, 1968.
(25) Kano, K.; Konse, T.; Uno, B.; Kubota, T. In *Redox Chemistry and Interfacial Behavior of Biological Molecules*; Dryhurst, G., Niki, K., Eds.; Plenum Press: New York, 1987; p 267.

rpm, suggesting that the electron transfer is a mass-transfer-controlled process. A diffusion coefficient of 5.3×10^{-6} cm^2 s^{-1} was estimated for both $[Cu^{II}(TTCN)_2]$ and $[Cu^{I}(TTCN)_2]$.

The number of electrons (n) involved in this redox process was calculated to be unity from the exhaustive electrolysis of 0.026 mmol of $[Cu^{II}(TTCN)_2]$ at a constant potential of 200 mV. The electrolysis was carried out at a glassy carbon RDE at 1600 rpm until the current decayed to <0.5% of the initial current.

The above electrochemical behavior can be accounted for in terms of a quasi-reversible one-electron process corresponding to the following redox reaction:

$$[Cu^{II}L_2] + e^- \rightleftarrows [Cu^{I}L_2] \qquad (1)$$

The cyclic voltammetric data are indicative of almost strict adherence to a simple one-electron-transfer process, as indicated by the close fit of the experimental and digitally simulated voltammograms of Figure 2. Digital simulation of the voltammetric data for the kinetic and thermodynamic parameters of the redox process corresponding to eq 1 was carried out by using a curve-fitting method. The formal redox potential ($E^{\circ\prime}_1$), the heterogeneous rate constant (k_{sh1}), and the cathodic-electron-transfer coefficient (α_1) were adjusted to give the best fit to the voltammograms. The independent analysis of 10 voltammograms at $v = 5 - 1000$ mV s^{-1} resulted in $E^{\circ\prime}_1 = 0.408 \pm 0.002$ V, $k_{sh1} = 0.0134 \pm 0.001$ cm s^{-1}, and $\alpha_1 = 0.45 \pm 0.04$. The refined curves calculated with these values, however, failed to reproduce the experimental voltammograms run at scan rates higher than 1 V s^{-1}. A steady increase in the value of k_{sh1} was observed with increasing scan rate for $2 < v < 10$ V s^{-1}, above which, up to a 30 V s^{-1} scan rate, a constant value of 2.3×10^{-2} cm^{-1} was obtained from the digital simulation. This behavior is indicative of a transition between two different rate-limiting processes.

It will be necessary to account for the changes in coordination geometry associated with electron transfer. If the redox-state-linked conformational changes are rapid and/or if the resulting species have redox potentials similar to those of the primary redox products, then it may not be possible to detect these conformational equilibria. Several additional electrochemical experiments were conducted to clarify this point. The kinetic parameters obtained for the electron-transfer step from double-step chronocoulometric experiments[26] over the range $5 < \tau \leq 100$ ms are in close agreement with those obtained from the CV data. However, the data obtained at $\tau = 5$ ms are indicative of a follow-up chemical step with a homogeneous rate constant of 470 s^{-1}, which would be quite fast on the CV time scale.

The i–E data for the RDE at 100 rpm plotted as log $(i/(i_l - i))$ vs electrode potential for both the oxidation of $[Cu^{I}(TTCN)_2]$ and the reduction of $[Cu^{II}(TTCN)_2]$ yielded straight lines with a theoretical Nernst slope of 59 mV and a half-wave potential of 408 mV, in exact agreement with cyclic voltammetric data. However, when the rotation speed is increased from 100 to 1600 rpm, a decrease of 10 mV is observed in the formal potential corresponding to the reduction of $[Cu^{II}(TTCN)_2]$, while an increase of essentially the same amount is observed in the oxidation of $[Cu^{I}(TTCN)_2]$, amounting to a total difference in the formal potentials of 20 mV. The slopes of the log plots corresponding to different rotation speeds remain essentially constant with a slight increase at high rotation speeds. While this difference in formal potentials may be due to the finite electron-transfer rate or uncompensated solution resistance, it is more likely attributable to the fact that the one-electron oxidation and the corresponding reduction do not involve the same species.

It is unlikely that uncompensated resistance in the aqueous medium employed will affect determination of the heterogeneous rate constant. The effect of the uncompensated resistance would be a decreased k_{sh1} at higher scan rates whereas the results from CV data, RDE, and chronocoulometry all indicate the contrary. Similarly, in the presence of significant uncompensated resistance, k_{sh1} will decrease with increasing concentration. The thermodynamic and kinetic parameters calculated from digital simulations for the $[Cu^{II/I}(TTCN)_2]$ complex did not depend on the concentration.

Scheme I. Proposed Square Mechanism for the Electron-Transfer Reaction of the $[Cu^{II/I}(TTCN)_2]$ System

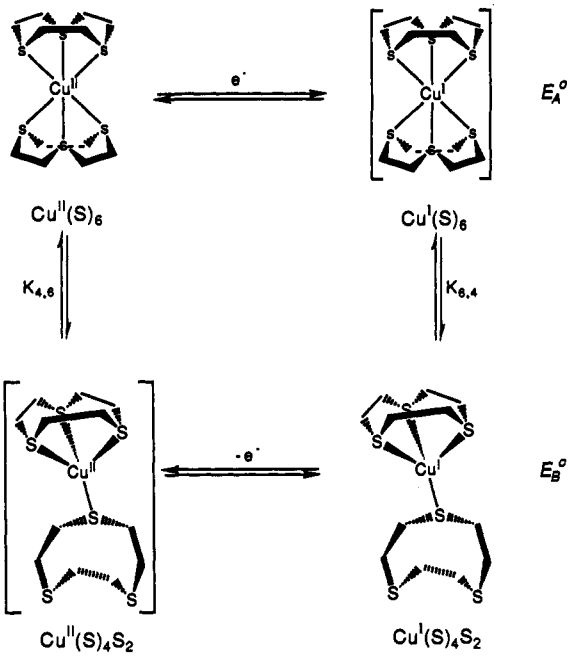

The negative shift in the formal potential corresponding to the reduction of $[Cu^{II}(TTCN)_2]$ with increasing rotation speed is indicative of the generation of an intermediate species (possibly octahedral Cu(I)) which is less stable than the final product, demonstrated to be tetrahedral Cu(I). Similarly, the positive shift in the formal potential corresponding to the oxidation of $[Cu^{I}(TTCN)_2]$ indicates a preference for octahedral Cu(II). These observations suggest a complex mechanistic pathway for the electron transfer. Accordingly, we propose the square mechanism outlined in Scheme I. A similar mechanism has already been proposed for the $Cu^{II/I}([14]aneS_4)$ system.[27,28]

Relatively slow scan rates provide sufficient time for the reduced complex to undergo the structural changes consistent with the coordination geometry requirements of Cu(I). This not only will result in the ligand dissociation but also would induce conformational changes in the partially dissociated macrocyclic ligand. Thus, the product of the reduction process, being a structurally different species, should be electrochemically different from the oxidized form. However, the redox potentials of the two copper complexes in different oxidation states are apparently too close to be resolved, and one can only see the time-averaged voltammograms of the entire system.

The observed values of the formal potentials and their dependence on the rotation speed can also be explained thermodynamically by considering the following two limiting cases both for the reduction of $[Cu^{II}(TTCN)_2]$ and for the oxidation of $[Cu^{I}(TTCN)_2]$ such that no kinetic complications are involved. (i) The system is completely electrochemically controlled, and no structural readjustment is involved on the time scale of the experiment. (ii) The time scale of the experiment is such that the system is chemically controlled and complete equilibrium is achieved.

Subscripts oct and tet will be used to represent octahedral and tetrahedral coordination geometries respectively, whereas square brackets in the equations will represent the bulk concentrations of the corresponding species; subscripted concentrations will represent the electrode surface concentrations. The reduction of $[Cu^{II}(TTCN)_2]$ can be treated thermodynamically as follows:

(26) Christie, J. H. *J. Electroanal. Chem. Interfacial Electrochem.* **1967**, *13*, 79.

(27) Bernardo, M. M.; Schroeder, R. R.; Rorabacher, D. B. *Inorg. Chem.* **1991**, *30*, 1241.

(28) Bernardo, M. M.; Robandt, P. V.; Schroeder, R. R.; Rorabacher, D. B. *J. Am. Chem. Soc.* **1989**, *111*, 1224.

$$[Cu^{II}L_2]_{oct} + e^- \overset{E^{\circ\prime}_A}{\rightleftharpoons} [Cu^{I}L_2]_{oct} \quad (2)$$

The Nernst equation corresponding to eq 2 can be written as eq 3. The chemical step following the electrochemical reduction

$$E_A = E^{\circ\prime}_A + (RT/F) \ln \{[Cu^{II}L_2]_{0,oct}/[Cu^{I}L_2]_{0,oct}\} \quad (3)$$

of $[Cu^{II}(TTCN)_2]$ can be represented by the following equilibrium process:

$$[Cu^{I}L_2]_{oct} \overset{K_{6,4}}{\rightleftharpoons} [Cu^{I}L_2]_{tet} \quad (4)$$

The equilibrium constant $K_{6,4}$ can be expressed as

$$K_{6,4} = [Cu^{I}L_2]_{tet}/[Cu^{I}L_2]_{oct} \quad (5)$$

The overall reduction process can be represented as eq 6 and the

$$[Cu^{II}L_2]_{oct} + e^- \overset{E^{\circ\prime}_1}{\rightleftharpoons} [Cu^{I}L_2]_{tet} \quad (6)$$

$$E_1 = E^{\circ\prime}_1 + (RT/F) \ln \{[Cu^{II}L_2]_{0,oct}/[Cu^{I}L_2]_{0,tet}\} \quad (7)$$

corresponding Nernst equation as eq 7. By combining eqs 3, 5, and 7, it can now be shown for the reduction process that

$$E^{\circ\prime}_1 = E^{\circ\prime}_A + (RT/F) \ln K_{6,4} \quad (8)$$

Similarly, the following relationship can be established for the oxidation of $[Cu^{I}(TTCN)_2]_{tet}$:

$$E^{\circ\prime}_2 = E^{\circ\prime}_B - (RT/F) \ln K_{4,6} \quad (9)$$

where $E^{\circ\prime}_A$ and $E^{\circ\prime}_B$ represent the formal potentials for the reduction of $[Cu^{II}(TTCN)_2]$ and oxidation of $[Cu^{I}(TTCN)_2]$, respectively, which do not include any structural readjustments. $E^{\circ\prime}_1$ and $E^{\circ\prime}_2$ are the formal potentials for the corresponding reduction and oxidation processes, including the coupled conformational changes. When complete chemical equilibrium is achieved, $E^{\circ\prime}_1$ and $E^{\circ\prime}_2$ must be equal. Moreover, in view of the stereochemical preferences of Cu(II) and Cu(I), it is safe to assume that $K_{6,4}$ and $K_{4,6} \gg 1$. It is obvious from the above treatment that the formal potential $E^{\circ\prime}_1$, corresponding to the reduction process where complete equilibrium is achieved, should be more positive than $E^{\circ\prime}_A$. In the case of oxidation, $E^{\circ\prime}_2$ should be smaller than $E^{\circ\prime}_B$.

The closeness of the two redox potentials, $E^{\circ\prime}_A$ and $E^{\circ\prime}_B$, can be explained by considering the chemical steps following the electron transfer as intermolecular reactions involving ligand dissociation equilibria[29] between Cu(I) and the sulfur atoms of its monodentate TTCN ring. The high restoring force of the endodentate conformation and the proximity of the dissociated sulfurs to the copper ion would tend to make the effective concentration of the ligand sufficiently high to keep the equilibrium to the left. This ligand-rich inner sphere would anchimerically favor faster ligand binding.[30] The crowding of the ligand about Cu(I), a d^{10} transition metal ion, would destabilize the system so as to favor Cu(II), which can accommodate a coordination number of 6.[31] However, sulfur, being a soft base, has greater affinity for Cu(I) than Cu(II) and, therefore, the Cu(I) oxidation state would be favored. An interplay among the ring-size effect, the macrocyclic effect, and the electronic effect is apparently responsible for such anomalous electrochemistry.

Electrochemistry of $[Cu^{II}(TTCN)_2]$ in the Presence of $Cu^{II}(aq)$. Cyclic voltammetry, RDE, and chronocoulometry results are all suggestive of conformational changes following electron transfer as outlined in Scheme I. The conformational readjustment imposed upon the complex by the oxidation state of the copper ion can however be stabilized, at least momentarily, by introducing an appropriate metal ion into the solution. Thus, the electrochemical studies of the system were carried out in an aqueous medium in the presence of different concentrations of added Cu(II).

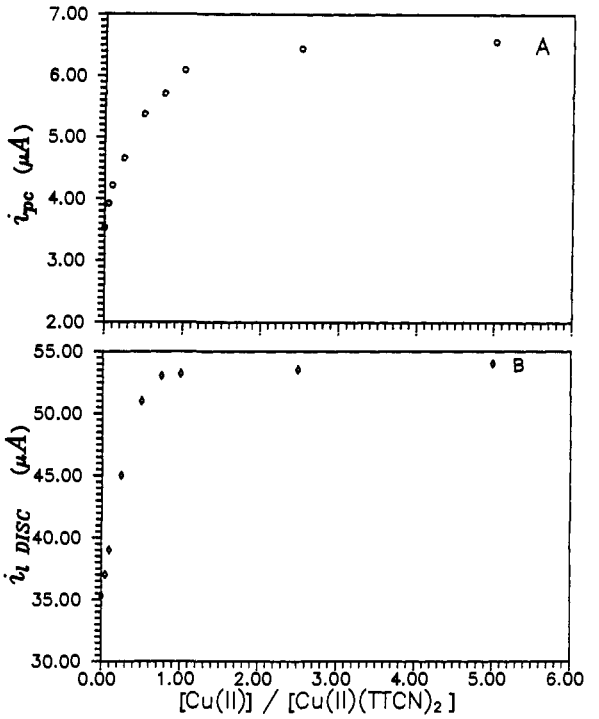

Figure 3. Titration of 1 mM $[Cu^{II}(TTCN)_2]$ with Cu(II) as a function of the ratio of $[Cu(II)]/[Cu^{II}(TTCN)_2]$: (A) CV cathodic peak current (i_{pc}); (B) limiting disc current ($i_{l\,DISC}$).

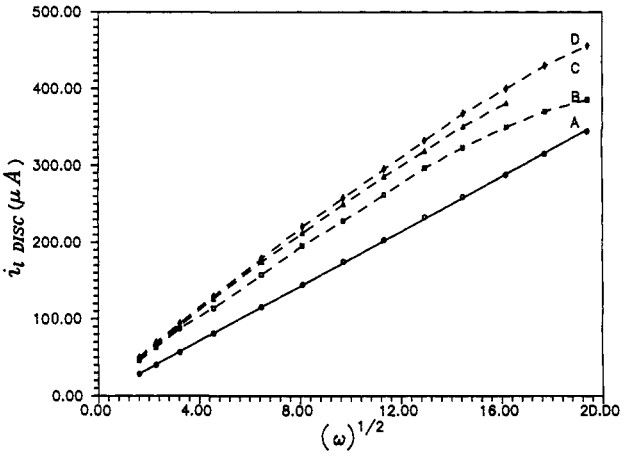

Figure 4. Plots of the limiting current vs $\omega^{1/2}$ for 1.0 mM $[Cu^{II}(TTCN)_2]$: (A) no added Cu(II); (B) 1 mM Cu(II); (C) 2.5 mM Cu(II); (D) 5 mM Cu(II).

Cu(II) is much harder to reduce than the complex (reduction of $Cu^{II}(aq)$ occurs below 0.120 V) and, therefore, does not interfere or overlap with the electrochemistry of the complex. Passing to the right across the first row of Figure 1 (increasing added Cu(II)), the cyclic voltammograms gradually become sharper and increase in height. The separation between the cathodic and anodic peaks narrows, and the apparent half-wave potential gradually shifts to more positive values, but the process remains essentially reversible. A plot of the cathodic peak current (i_{pc}) vs the ratio $[Cu(II)]/[Cu^{II}(TTCN)_2]$ results in a linear increase in the peak current initially which finally levels off at a value of 1.842 times that of the complex alone (Figure 3A). This value is very close to the theoretical value of 1.837 ($n^{3/2}$) for a reversible electron-transfer step of 1.5 electrons.[32] The inflection point corresponds

(29) Geiger, W. E. In *Progress in Inorganic Chemistry*; Lippard, S. J., Ed.; John Wiley: New York, 1985; Vol. 33, p 275.
(30) Hartman, J. R.; Cooper, S. R. *J. Am. Chem. Soc.* **1986**, *108*, 1202.
(31) Brill, A. S.; Martin, R. B.; Williams, J. P. In *Electronic Aspects of Biochemistry*; Pullman, B., Ed.; Academic Press: New York, 1964; p 519.
(32) Bard, A. J.; Faulkner, L. R. *Electrochemical Methods: Fundamentals and Applications*; Wiley: New York, 1980.

to a concentration ratio of 0.5. Similarly, from the RDE experiments, a plot of the limiting current ($i_{l\,DISC}$) vs the concentration ratio resulted in a current ratio of 1.5 and concentration ratio of 0.5 at the inflection point (Figure 3B).

The total number of electrons involved in the overall reduction process of the mixture was determined from the CPE of 0.025 mmol of $[Cu^{II}(TTCN)_2]$ in the presence of 0.13 mmol of Cu(II) at 200 mV. The electrolysis resulted in an "*n*" value of 1.45, which compares with the theoretical value of 1.5.

Figure 4 shows the Levich plots corresponding to the reduction of 1 mM $[Cu^{II}(TTCN)_2]$ with varying concentrations of Cu(II). The initial slopes of the plots for the mixtures are characteristic of 1.5 electrons, but at high rotation speed, depending on the relative concentration of Cu(II), the slopes decrease and converge with the Levich plot for the simple reduction of $[Cu^{II}(TTCN)_2]$. The same dependence of the plots of $i_{l\,RING}$ vs $\omega^{1/2}$ on [Cu(II)]/$[Cu^{II}(TTCN)_2]$ was seen. Thus, changing the time scale of the experiment illustrates the influence of the following chemical reaction. At high scan rates (Figure 1, row 4), it is also possible to observe the partial resolution of the consecutive one-electron steps.

These results support the reaction resulting in the formation of the trinuclear complex, shown as follows:

$$2ML + Cu(II) \underset{}{\overset{K_1}{\rightleftharpoons}} [Cu^{II}(ML)_2] \quad (ML = [Cu^{I}(TTCN)_2]) \tag{10}$$

The corresponding equilibrium constant can be expressed as

$$K_1 = [Cu^{II}(ML)_2]/\{[Cu(II)][ML]^2\} \tag{11}$$

The trinuclear complex ($[Cu^{II}(ML)_2]^{4+}$) then undergoes a one-electron reduction at the electrode surface at a potential more positive than the formal potential of $[Cu^{II}(TTCN)_2]$:

$$[Cu^{II}(ML)_2] + e^- \overset{E^{\circ\prime}_3}{\rightleftharpoons} [Cu^{I}(ML)_2] \tag{12}$$

The Nernst equation for eq 12 can be written as

$$E_3 = E^{\circ\prime}_3 + (RT/F) \ln \{[Cu^{II}(ML)_2]_0/[Cu^{I}(ML)_2]_0\} \tag{13}$$

For the sake of simplicity, in addition to the assumption that $K_{6,4} \gg 1$, we further assume that the presence of Cu(II) in solution would shift the equilibrium further to the right such that only eq 6 can be considered as an electrochemical step preceding the chemical reaction between $[Cu^{I}(TTCN)_2]$ and Cu(II). Slow scan rates provide sufficient time for the processes of eq 10 to attain equilibrium, thus ensuring complete chemical reversibility. The observations that only one redox process is evident for any composition of the test solution and that the positive shift in the peak potentials coupled with decreased peak separation (ΔE) and increased i_p's with increasing Cu(II) concentration suggest that the formal potential for the redox process of eq 12 ($E^{\circ\prime}_3$) should be more positive than $E^{\circ\prime}_1$ of eq 6. Therefore, for a sufficiently positive $E^{\circ\prime}_3$ relative to $E^{\circ\prime}_1$ and with excess Cu(II) present, a one-step reduction (n = 1.5 electrons) is expected for the redox process:

$$2[Cu^{II}L_2] + Cu(II) + 3e^- \overset{E^{\circ\prime}_4}{\rightleftharpoons} [Cu^{I}(ML)_2] \tag{14}$$

For a relatively higher scan rate and lower Cu(II) concentration, e.g. the bottom row of Figure 1, the process is dominated by the electron transfer: the chemical interactions do not have sufficient time to take place, and only the simple one-electron reduction of $[Cu^{II}(TTCN)_2]$ is observed.

Digital simulation, based on an ECE mechanism, failed to closely reproduce the experimental curves. This indicates that some other process might also be operative. It can be assumed that the chemical step following the first electron-transfer step is not a diffusion-limited reaction. Therefore, some $[Cu^{I}(TTCN)_2]$ produced at the electrode surface can diffuse into the solution before interacting with the free copper at the electrode surface and produce the trinuclear complex in solution according to eq 10. This complex can then diffuse back to the electrode and undergo electrochemical reduction. At the same time, the complex can undergo solution electron transfer with the diffusing $[Cu^{I}(TTCN)_2]$ according to eq 15. In that case, K_2 must also be

$$[Cu^{I}(L)_2] + [Cu^{II}(ML)_2] \overset{K_2}{\rightleftharpoons} [Cu^{I}(ML)_2] + [Cu^{II}L_2] \tag{15}$$

considered in the calculation of the corresponding kinetic and thermodynamic parameters.

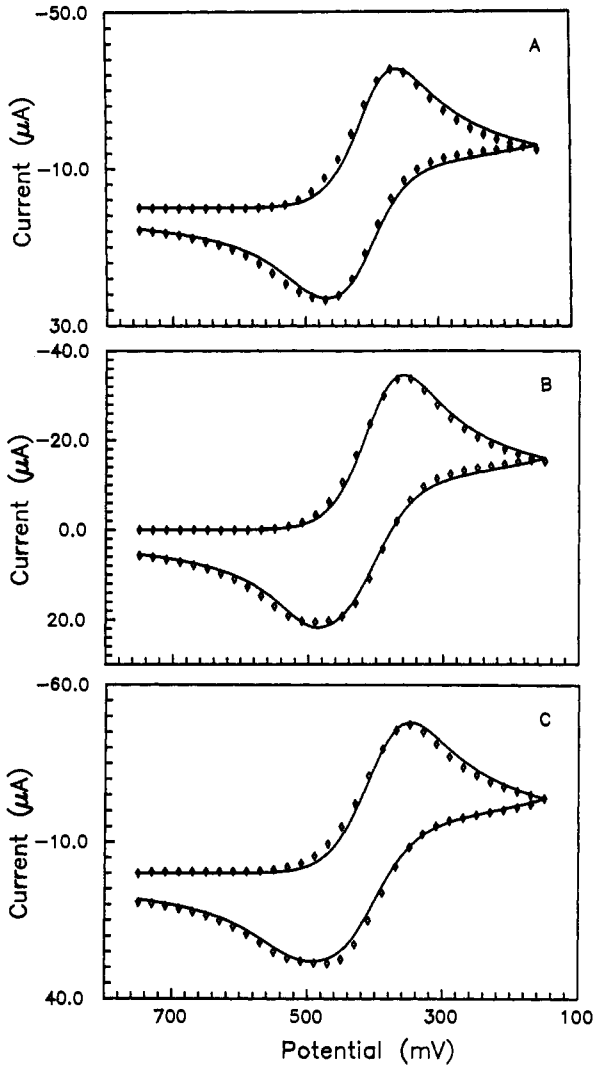

Figure 5. Background-corrected experimental (◇◇◇) and corresponding digitally simulated (—) cyclic voltammograms of 1.0 mM $[Cu^{II}(TTCN)_2]$ in the presence of (A) 0.05 mM added Cu(II) at v = 0.500 V s^{-1}, (B) 0.1 mM added Cu(II) at v = 0.500 V s^{-1}, and (C) 0.1 mM added Cu(II) at v = 1.000 V s^{-1}. $E^{\circ\prime}_3 \approx 0.60$ V, $\alpha_3 \approx 0.5$, and $k_{sh3} \approx 0.01$ cm s^{-1}.

When eq 15 was included in the simulation program, the analysis of five voltammograms at different scan rates and Cu(II) concentrations reproduced very closely the experimental voltammograms, as shown in Figure 5.

Because of the complex nature of the proposed follow-up chemical reaction, represented by eq 10, no direct theoretical analysis of the i–E curves was attempted. However, the digital simulation was carried out first for the apparently reversible slow scan rate voltammograms of a number of mixture compositions. It was assumed that a 5 mV s^{-1} scan rate is slow enough to allow the follow-up chemical reaction to attain equilibrium. Fixing the electrochemical parameters already determined for the redox process preceding the chemical step of eq 10, preliminary calculations indicated that the generated i–E curves at a given K_1K_2 were practically independent of K_2 as long as $K_2 > 10$, which would be the case when $(E^{\circ\prime}_3 - E^{\circ\prime}_1) > 60$ mV. This may be ascribed to the statistical correlation between K_1 and K_2. Since the independnt estimation of K_1K_2 is difficult, therefore, the adjustment

of K_1K_2 was allowed to get the best fit. For the digital simulation, the diffusion coefficients were set as $D_1 = D_2 = 5.3 \times 10^{-6}$, $D_3 = D_4 = 4.6 \times 10^{-6}$, and $D_{Cu(II)} = 7.0 \times 10^{-6}$ cm^2 s^{-1}, where D_1, D_2, D_3, and D_4 are the diffusion coefficients of $[Cu^{II}L_2]$, $[Cu^{I}L_2]$, $[Cu^{II}(ML)_2]$, and $[Cu^{I}(ML)_2]$, respectively. In this way, the analysis gave $K_1K_2 = 5.87 \times 10^7$ M^{-2}.

It is obvious from Figure 1 that the shape of the cyclic voltammograms depends strongly on both the relative concentration of added Cu(II) and the scan rate. The changes associated with these parameters can be explained in terms of the kinetics of the electron transfer (eqs 1 and 12) and the follow-up chemical step (eq 10). Our model specifies that the solution electron-transfer reaction of eq 15 is in equilibrium on the time scale of relatively slower scan rates ($v < 2$ V s^{-1}).

The kinetic and thermodynamic parameters corresponding to eqs 10 and 12 were calculated from the digital simulation. This was done by adjusting the electron-transfer rate constant (k_{sh3}), the cathodic-transfer coefficient (α_3), and $E^{\circ\prime}{}_3$ corresponding to the redox process of eq 12 and the forward rate constant (k_f) corresponding to eq 10. In this way, the values obtained are $E^{\circ\prime}{}_3 \approx 0.60$ V, $\alpha_3 \approx 0.5$, $k_{sh3} \approx 0.01$ cm s^{-1}, and $k_f \approx 2 \times 10^8$ M^{-2} s^{-1}. The validity and consistency of these values is manifested in the close fit of the calculated curves with the experimental voltammograms. The set of estimated values of various constants can explain the entire spectrum of voltammograms at $v < 2$ V s^{-1} shown in Figure 1.

Potentiometric Analysis. Based on the proposed mechanisms, a mathematical analysis can be carried out for the potentiometric titration of $[Cu^{I}(TTCN)_2]$, generated at the electrode surface, with Cu(II).

Comparing eqs 10 and 7, it is obvious that the effect of adding free copper to the solution is a progressive shift of the apparent formal potential of the process to a more positive value until the equilibrium is driven completely to the right at high concentrations of added copper. The value of such a limiting formal potential can mathematically be predicted by correlating $E^{\circ\prime}{}_4$ of eq 14 with K_1.

Under the conditions that $[Cu(II)] \gg [Cu^{II}(TTCN)_2]/2$ and $K_1 \gg 1$, the complex $[Cu^{II}(TTCN)_2]$ would be almost completely converted to $[Cu_3(TTCN)_4]^{3+}$ at the electrode surface upon reduction at low scan rates. The Nernst equation for eq 14 can then be written as eq 16.

$$E_4 = E^{\circ\prime}{}_4 + (RT/3F) \ln \{([Cu^{II}L_2]_0)^2[Cu(II)]/[Cu^{I}(ML)_2]_0\} \quad (16)$$

Equations 7, 11, 13, and 16 can be combined to obtain eq 17 for the limiting value of the formal potential corresponding to eq 14 under complete formation of $[Cu_3(TTCN)_4]^{4+}$ (eq 10).

$$E^{\circ\prime}{}_4 = \{(2E^{\circ\prime}{}_1 + E^{\circ\prime}{}_3)/3\} + (RT/3F) \ln (K_1) \quad (17)$$

However, when [Cu(II)] is not very high compared to $[Cu^{II}(TTCN)_2]$, eq 15 cannot be ignored. The equilibrium constant corresponding to eq 15 can be represented as

$$K_2 = \{[Cu^{II}L_2][Cu^{I}(ML)_2]\}/\{[Cu^{II}(ML)_2][Cu^{I}L_2]\} = \exp[(F/RT)(E^{\circ\prime}{}_3 - E^{\circ\prime}{}_1)] \quad (18)$$

Taking the solution electron transfer into account, eq 16 can be modified to eq 19.

$$E^{\circ\prime}{}_4 = E^{\circ\prime}{}_1 + (RT/3F) \ln (K_1K_2) \quad (19)$$

Under the conditions that $[Cu(II)]_0 \approx [Cu(II)]_{eq} \approx [Cu(II)]$, where the subscript "eq" represents the equilibrium concentration, the following equation for the potentiometric titration can be obtained:

$$E^{\circ\prime}{}_{app} = E^{\circ\prime}{}_1 + (RT/3F) \ln (K_1K_2[Cu(II)][Cu^{II}L_2]) \quad (20)$$

where $E^{\circ\prime}{}_{app} \equiv E^{\circ\prime}{}_4 + (RT/3F) \ln ([Cu^{II}(TTCN)_2][Cu(II)])$ is an apparent formal potential for a particular composition of the mixture and will have the same numerical value as the electrode potential at half-reduction when $[Cu^{II}L_2]_0 = [Cu^{II}(TTCN)_2]/2$ and $[Cu^{I}(ML)_2]_0 = [Cu^{II}(TTCN)_2]/4$.

Scheme II. Proposed Mechanism for the Heterogeneous Electron Transfer of $[Cu^{II}(TTCN)_2]$ Followed by Interaction with Free Cu(II) and Subsequent Electron Transfer of the Proposed Intermediate Trinuclear Complex

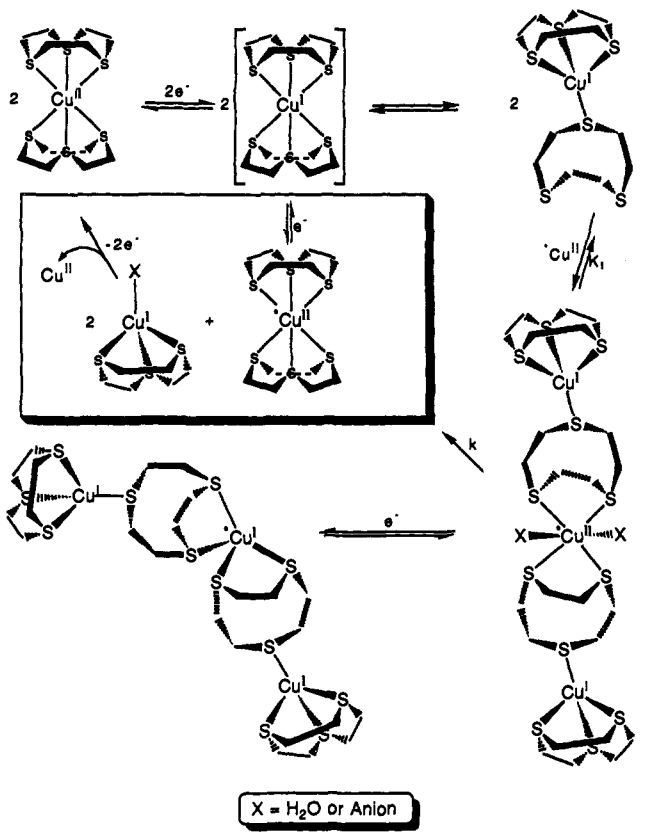

Polarographic half-wave potentials corresponding to the electron-transfer steps defined by eqs 6 and 14 can be represented by eqs 21 and 22, respectively. Combining eqs 20–22 will give

$$E_{1/2,1} = E^{\circ\prime}{}_1 + (RT/2F) \ln (D_2/D_1) \quad (21)$$

$$E_{1/2,app} = E^{\circ\prime}{}_{app} + (RT/6F) \ln (D_4/D_1) \quad (22)$$

eq 23. When $D_1 = D_2$, which is the case here, then eq 23 can

$$E_{1/2,app} - E_{1/2,1} = (RT/3F)\{\ln (K_1K_2[Cu^{II}L_2][Cu(II)]) + \ln (D_4D_1{}^2/D_2{}^3)/2\} \quad (23)$$

further be simplified to obtain eq 24 for the potentiometric analysis of the voltammetric data.

$$E_{1/2,app} - E_{1/2,1} = (RT/3F)\{\ln (K_1K_2[Cu^{II}L_2][Cu(II)]) + \ln (D_4/D_1)^{1/2}\} \quad (24)$$

The values of $E_{1/2,app}$ were estimated as $(E_{pa} + E_{pc})/2$ for the apparently reversible voltammograms run at $v = 5$ mV s^{-1}. A plot of $(E_{1/2,app} - E_{1/2,1})$ vs log ([Cu(II)]) affords a straight line with a slope of 16.8 mV in the range when $[Cu(II)]/[Cu^{II}(TTCN)_2] \approx 0.25$–$0.75$. This is somewhat smaller than the theoretical value of 19.7 mV. While this difference can be ascribed to the assumption concerning $[Cu(II)]_0$ and $[Cu(II)]_{eq}$, the possibility of further formation of other copper complexes at much higher Cu(II) concentrations cannot be ruled out. Moreover, for a complete and successful theoretical analysis, a detailed knowledge of the kinetics and thermodynamics of the decomposition of the trinuclear complex (Scheme II) is needed. The existence of this competing chemical process has been strongly supported by our preliminary results with some other Cu(I)–TTCN systems. These studies have also indicated that the decomposition product $[Cu^{I}(TTCN)X]$ (X = H_2O, A^-) has about the same redox potential as that calculated for the trinuclear complex, which makes

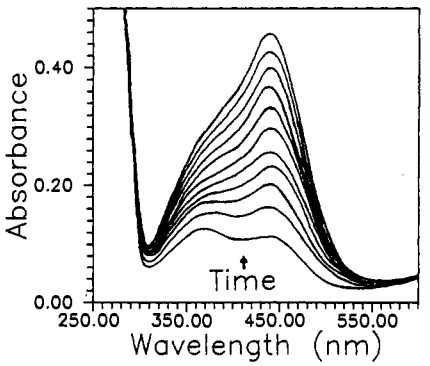

Figure 6. Selected electronic spectra of a 5:1 mixture of [Cu(II)] and $[Cu^{II}(TTCN)_2]$ recorded after electrolysis to about 3% of the initial current at zero time and after every 3 h. (These spectra are selected from a number of spectra recorded at 30-min intervals after the electrolysis.)

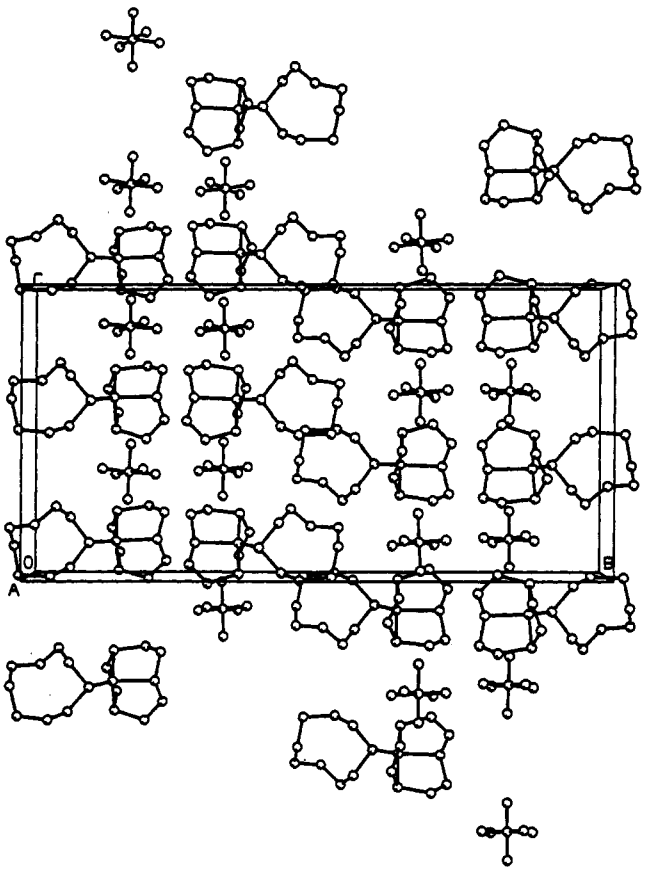

Figure 7. Packing of the unit cell of $[Cu(TTCN)_2]PF_6$.

the two pathways electrochemically indistinguishable from each other.[33]

Spectral Analysis. The electronic spectrum of $[Cu^{II}(TTCN)_2]$ over the range 850–300 nm gives a single symmetrical peak centered at 444 nm. No change in the spectral behavior of $[Cu(TTCN)_2]^{2+}$ over a period of 24 h at room temperature was observed upon titration with Cu(II). A mixture, 2 mM in $[Cu^{II}(TTCN)_2]$ and 10 mM in Cu(II), was electrolyzed at 200 mV until the current decayed to about 3% of the initial current. The spectrum of the electrolyzed mixture was run immediately after the electrolysis (Figure 6). The appearance of a new peak at 370 nm, where there is no absorbance from the free copper or the $[Cu^{II}(TTCN)_2]$ complex, is a clear indication of the production of a new species. The peak at 440 nm can be ascribed to the absorption due to the unelectrolyzed $[Cu^{II}(TTCN)_2]$ and the 370-nm peak to the trinuclear complex. The 370-nm peak of the electrolyzed mixture appears almost at the same position as the

(33) Sanaullah; Wilson, G. S. Unpublished data.

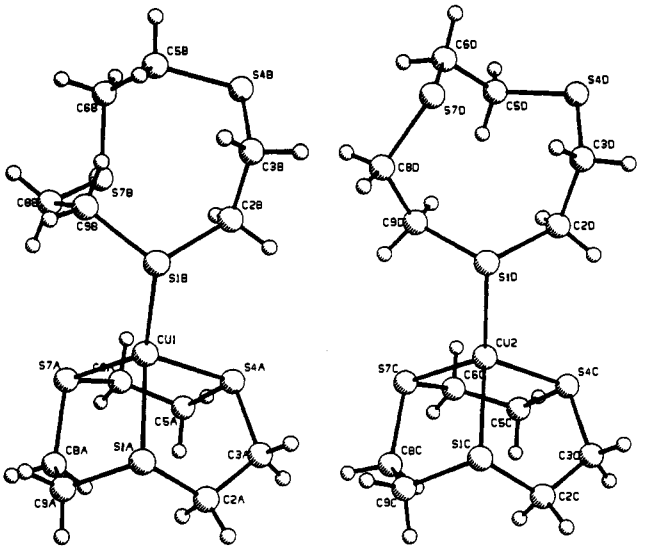

Figure 8. Structures of the two molecular units of the unit cell in Figure 7.

Table II. Selected Geometrical Parameters for $[Cu(TTCN)_2]PF_6$

A. Intramolecular Distances (Å)			
Cu1–S1A	2.332 (6)	Cu2–S1C	2.288 (7)
Cu1–S4A	2.327 (5)	Cu2–S4C	2.317 (6)
Cu1–S7A	2.300 (6)	Cu2–S7C	2.334 (7)
Cu1–S1B	2.224 (6)	Cu2–S1D	2.246 (6)
B. Intramolecular Bond Angles (deg)			
S1A–Cu1–S4A	92.9 (2)	S1C–Cu2–S4C	94.5 (2)
S1A–Cu1–S7A	93.4 (2)	S1C–Cu2–S7C	94.0 (2)
S1A–Cu1–S1B	117.0 (2)	S1C–Cu2–S1D	120.5 (2)
S4A–Cu1–S7A	94.0 (2)	S4C–Cu2–S7C	93.6 (2)
S4A–Cu1–S1B	119.4 (2)	S4C–Cu2–S1D	122.8 (2)
S7A–Cu1–S1B	131.2 (2)	S7C–Cu2–S1D	123.8 (2)
C. Torsion Angles of the Monodentate TTCN Ring (deg)			
S1B–C2B–C3B–S4B	−122 (2)	C3B–S4B–C5B–C6B	−103 (2)
S4D–C3D–C2D–S1D	−122 (1)	C2D–S1D–C9D–C8D	−102 (2)
S1B–C9B–C8B–S7B	−61 (2)	S4B–C5B–C6D–S7B	54 (3)
S4D–C5D–C6D–S7D	−60 (2)	S1D–C9D–C8D–S7D	57 (2)
C2B–S1B–C9B–C8B	76 (2)	C5B–C6B–S7B–C8B	79 (2)
C3D–S4D–C5D–C6D	76 (2)	C9D–C8D–S7D–C6D	73 (2)
C2B–C3B–S4B–C5B	85 (2)	C6B–S7B–C8B–C9B	−79 (2)
C3D–C2D–S1D–C9D	83 (2)	C8D–S7D–C6D–C5D	−78 (2)
C3B–C2B–S1B–C9B	60 (2)		
C2D–C3D–S4D–C5D	58 (2)		

peak assigned to the $S(\sigma) \rightarrow Cu(II)$ charge transfer for copper(II)–thioether complexes of the form $[Cu^{II})L]$ where L = [12]-aneS$_4$, [13]aneS$_4$, and [14]aneS$_4$.[27,34]

The increase in the intensity of the 440-nm peak with time (Figure 6) indicates the regeneration of the original complex either by the decomposition of the trinuclear complex or through autoxidation, however most likely the former. Moreover, the completely reduced trinuclear complex, supposing that all the copper centers have tetrahedral geometry, could be subject to high steric repulsion, which would allow it to be easily attacked by the Cu(II) ion, leading to the regeneration of the $[Cu^{II}(TTCN)_2]$ complex.

Crystallographic Analysis. $[Cu(TTCN)_2]PF_6$ crystallizes in space group $P2_1/n$ of the monoclinic system with two formula units per unit cell. Packing of the unit cell is shown in Figure 7. The two molecular units in the unit cell differ from each other mainly in the ligation of the monodentate TTCN ligand although the conformation of these ligands is the same (Figure 8).

The conformation of the monodentate ligand is substantially different from the [1 2 2 2 2] conformation observed in the mon-

(34) Jones, T. E.; Rorabacher, D. B.; Ochrymowycz, L. A. *J. Am. Chem. Soc.* **1975**, *97*, 7485.

odentate ring in $[Au(TTCN)_2]PF_6$,[12] the bridging ring in $[Cu_2(TTCN)_3](BF_4)_2 \cdot H_2O$, and the commonly observed endodentate [3 3 3] conformation. It appears that TTCN is a more flexible ligand than previously suggested, but the relative importance of conformational constraints of the ligand in determining coordination geometry in metal complexes has not yet been fully clarified. The coordination about Cu(I) in both the molecular units represents a distorted tetrahedral geometry (Table II).

In any case, it is obvious from the torsion angles of the crystallographic data and Figure 8 that the uncoordinated sulfurs in the singly coordinated macrocycle are directed outward relative to the coordinated sulfur and are thus prone to attack by another appropriate metal ion. In order to effect the chelation, the macrocycle must undergo significant conformational changes which can jeopardize the bonding between the coordinated sulfur of the same ring and Cu(I). Further, the free 1,4,7-trithiacyclononane macrocycle prefers the endodentate conformation. Thus, the coordination of the two dissociated sulfurs to another transition metal ion forces the third and Cu(I)-coordinated sulfur to move toward an endodentate [3 3 3] conformation regardless of whether there is a strong interaction between this sulfur and the newly coordinated metal ion. This effect was seen when $[Cu(TTCN)_2]PF_6$ was reacted with nickel(II), cobalt(II), and palladium(II), yielding $[Ni^{II}(TTCN)_2]$, $[Co^{II}(TTCN)_2]$, and $[Pd^{II}(TTCN)_2]$ substitution products, respectively,[14,35] rather than the expected trinuclear complexes. Moreover, the instability of the trinuclear complexes can also be ascribed to nonbonded repulsive interactions.

Considering all of the above observations, we propose the following mechanism for the electron-transfer reactions of bis(1,4,7-trithiacyclononane)copper(II) in the presence of free copper (Scheme II).

The fact that the intermediate trinuclear complex has a relatively more positive redox potential ($E^{\circ\prime}_3$) compared with that of $[Cu^{II}(TTCN)_2]$ ($E^{\circ\prime}_1$) can be explained as follows. Cyclic thioethers tend to stabilize Cu(II) better than acyclic thioethers.[5] This tendency is more obvious in the case of TTCN because the sulfurs are rigidly preorganized for facial coordination. However, the greater affinity of Cu(I) for thioethers would cause the redox potential of $[Cu^{II}(TTCN)_2]$ to be relatively high compared with those of the ammine and oxo analogues[36] but not as high as those of the acyclic or more flexible macrocyclic thioethers.[7] In the trinuclear complex, the terminal $[Cu^{I}(TTCN)_2]$ units appear to behave as bidentate ligands for the central copper atom. The loss of the macrocyclic effect would result in a higher redox potential of the central copper; however, the rigidity of this bidentate ligand may be considered responsible for the relatively small shift. This coordination of the uncomplexed sulfur atoms of the $[Cu^{I}(TTCN)_2]$ complex provides further evidence that the geometry of this complex in solution is at least similar if not the same as that determined unequivocally in the solid state by X-ray crystallographic methods.

Concluding Remarks

It is important to reconcile the electrochemical data with the other chemical properties of the two copper oxidation states. The evidence for the formation of the trinuclear complex is unequivocal. The influence of conversion between $[Cu^{I}(TTCN)_2]_{oct}$ and $[Cu^{I}(TTCN)_2]_{tet}$ and that between $[Cu^{II}(TTCN)_2]_{tet}$ and $[Cu^{II}(TTCN)_2]_{oct}$ on the electrochemistry is less easy to discern. This is probably due to the rapidity of these reactions with respect to the electron transfer and the fact that the potentials coupled with the processes are different but closely spaced. At least for the oxidation of $[Cu^{I}(TTCN)_2]$, recent evidence from pulse radiolysis[33] suggests that the conformational change is not concerted, as a distinct $[Cu^{II}(TTCN)_2]_{tet}$ intermediate appears to exist.

The systems presented in this report are obviously quite complicated; however, the reliability of the proposed mechanisms lies in the fact that several alternative mechanisms, through digital simulation, failed to consistently reproduce the experimental curves. These alternative mechanistic schemes involved (i) no solution electron transfer, (ii) a direct two-electron oxidation of the trinuclear complex ($[Cu^{I}_2Cu^{II}(TTCN)_4]$) to two $[Cu^{II}(TTCN)_2]$ and a free Cu(II), or (iii) the generation of a dinuclear intermediate from the interaction between $[Cu^{I}(TTCN)_2]$ and Cu(II), followed by the formation of the trinuclear complex.

TTCN, once the most difficult crown thioether to synthesize, is now a commonplace compound. The research involving TTCN has surpassed that involving any of the other thioethers because of its unique nature. The angular restraints imposed by the smaller size of the ring keeps the TTCN molecule in a fairly rigid endodentate [3 3 3] conformation,[8,9] unlike the case of the other more flexible sulfur macrocycles. This makes TTCN an ideal ligand for facial coordination to a metal ion. The larger covalent radius of S compared to that of N would result in longer M–S and C–S bonds in complexes of S-crowns compared to the corresponding M–N and C–N bonds in complexes of N-crowns. Thus, the instability caused by the steric repulsions particularly between the two ligands of a $[M(TTCN)_2]$ molecule does not play as significant a role as in the analogous triaza complexes, $[M(TACN)_2]$.[37] The versatility of TTCN as a ligand can be ascribed to the favorable covalent radius of the sulfur atom, the unique ring character, the macrocyclic effect, and the electronic properties of the coordinating sulfur atoms.

Acknowledgment. We thank Dr. Fusao Takusagawa for his assistance in the X-ray crystallographic determination and the National Institutes of Health (Grant HL-15104) for financial support.

Supplementary Material Available: A table of positional parameters (4 pages); a listing of structure factors (38 pages). Ordering information is given on any current masthead page.

(35) Wieghardt, K.; Kuppers, H.-J.; Raabe, E.; Kruger, C. *Angew. Chem., Int. Ed. Engl.* **1986**, *25*, 1101.

(36) Root, M. J.; Sullivan, B. P.; Meyer, T. J.; Deutsch, E. *Inorg. Chem.* **1985**, *24*, 2731.

(37) Hancock, R. D. In *Progress in Inorganic Chemistry*; Lippard, S. J., Ed.; Wiley: New York, 1989; p 187.